The Astrophysical Journal, 614:922–928, 2004 October 20
© 2004. The American Astronomical Society. All rights reserved. Printed in U.S.A.

PROPAGATION AND TRANSMISSION OF ALFVÉN WAVES IN ROTATING MAGNETARS

Yasufumi Kojima and Taishi Okita
Department of Physics, Hiroshima University, Higashi-Hiroshima 739-8526, Japan; kojima@theo.phys.sci.hiroshima-u.ac.jp
Received 2004 January 5; accepted 2004 June 24

ABSTRACT

We study the propagation and transmission of Alfvén waves in the context of cylindrical geometry. This approximates the polar cap region of aligned pulsar with strong magnetic fields. Nonpropagating region appears in the presence of rotation. The displacement current further prevents the low-frequency modes from propagating near the stellar surface. The transmission rates to the exterior through the surface are calculated. The rates increase with the frequency and the magnetic field strength. The transmission also depends on the helicity states of the waves, but the difference becomes small in the high-frequency regime. We also point out the possibility of the spin-up by outgoing wave emission in the low-frequency regime if a certain condition holds.

Subject headings: gamma rays: bursts — stars: magnetic fields — stars: neutron

1. INTRODUCTION

Soft gamma repeaters (SGRs) and anomalous X-ray pulsars (AXPs) belong to a rare class among thousands of neutron stars. Both objects are different from so-far known neutron stars in their radiation spectrum and spin periods. SGR-like outbursts were also discovered in AXPs (Gavriil et al. 2002; Kaspi et al. 2003), and hence there are similarities between two peculiar neutron stars. They are likely to be young and isolated, but they have intense magnetic fields in the 10^{14}–10^{15} G range. See Mereghetti & Stella (1995) and Kouveliotou et al. (1998) for their initial observations and also Woods (2004) for recent reviews. Further evidence of the strong magnetic fields has recently come from spectral line features (Ibrahim et al. 2003). These objects are called magnetars (Thompson & Duncan 1993, 1995, 1996). The magnetar model can explain the peculiar observational properties (see, e.g., Thompson [2000] and Lyutikov et al. [2002] for recent reviews). The burst emission and nonthermal X-ray radiation are supplied by the decay of strong magnetic fields. Twisted magnetic fields relevant to the activities are transported from the core to the surface by ambipolar diffusion in the magnetars model (Thompson et al. 2002).

The Alfvén waves are likely to be excited by sudden disturbances in various magnetized objects. Short-duration bursts in SGRs may be associated with starquakes driven by magnetic stress, since similarities in the statistical properties of SGRs and earthquakes have been reported (Cheng et al. 1996; Göğüş et al. 1999, 2000). The properties and physical mechanism of Alfvén waves are very interesting. The fluid displacement is perpendicular to both the wave vector and the magnetic field, and a restoring force arises from the magnetic tension of the field lines. The plane Alfvén waves of finite amplitude can propagate at constant speed in a homogeneous incompressible medium without any distortion of the waveform. This contrasts with sound waves, which may steepen to form shocks because of the nonlinearity. As for the physical mechanism, torsional Alfvén waves can transport angular momentum and account for the spin-down of rotating objects such as magnetized stars with convective envelopes, interstellar clouds threaded by the Galactic magnetic fields, and so on (see, e.g., Shu 1992 for details.

In this paper we consider the Alfvén waves produced by shaking the magnetic field lines in a rotating magnetar. The origin of abrupt disturbances relevant to the bursts is not addressed here, but the subsequent propagation and ejection to the exterior are examined. The total energy in shorter duration bursts is $\Delta E < 10^{41}$ ergs and is a small fraction of the available magnetic energy, $\sim 10^{-5} E_B$, where the total magnetic energy E_B is estimated by the expected dipole field strength $B = 10^{14}$–10^{15} G. On the other hand, giant flares with $\Delta E \sim 10^{44}$ ergs should involve a change of the magnetic field configuration on a global scale (Ioka 2001; Woods et al. 2001). We here use linearized perturbation equations, which are applicable to less energetic events $\Delta E/E_B \propto (\delta B/B)^2 \ll 1$, in the shorter duration bursts. Our results of the wave propagation cannot be applied to the giant flares, but there may be some similarities in nature even for $\delta B \sim B$. The ejection of Alfvén waves to the exterior has already been estimated, but our model goes beyond this. We here explicitly calculate the transmission in a cylindrical geometry. We also calculate the energy and angular momentum extracted by the waves through the stellar surface. In § 2 we provide a geometrically simplified model. The propagation in the neutron star crust and transmission to the exterior can be examined in a concrete way with this simplified model. The shear in the solid crust acts as an additional restoring force. Therefore, "shear Alfvén waves" may be a more adequate name. The transmission rate is numerically calculated for the waves with higher frequency. We discuss the implications of our results in § 3.

2. ALFVÉN WAVES IN A ROTATING CYLINDER

2.1. *Model*

In this paper we study the propagation of shear Alfvén waves through a neutron star crust and their transmission to the exterior. The star is assumed to rotate around the z-axis with a constant angular velocity, Ω. The magnetic field is uniform along the z-axis, i.e., $\boldsymbol{B} = B_0 \boldsymbol{e}_z$, where B_0 is a constant. Our consideration is limited to a cylindrically symmetric slab region within the radius ϖ_*. The magnetic fields are rather easily incorporated in the cylindrical model. Carroll et al. (1986) studied the oscillation spectra of magnetized/unmagnetized cylindrical stars. Their results show that the periods of the torsional and shear modes are in good agreement with those of spherically symmetric unmagnetized stars. This suggests that the approximation is good for some modes.

The cylindrical approximation may be adequate for the polar cap region and the interior for an aligned rotator. In this

case, the radius ϖ_* is given by the size of the polar cap, $\varpi_* \leq R \sin\theta_p = (R^3\Omega/c)^{1/2} \approx 10^4 (T/1\ \mathrm{s})^{-1/2}$ cm, where $R \approx 10^6$ cm is stellar radius and T is the rotational period. The exterior magnetic field lines that originate from this region extend to infinity. On the other hand, the field lines outside the polar cap are closed. The plasma along the closed lines corotates with the central star. In our cylindrical model, we consider the shaking of open field lines only, which may lead to particle acceleration, magnetic reconnection, wind, and eventually to radiation. Explicit treatment of the energy transfer to the radiation is beyond the scope of this paper.

The shear stress in the crust also acts as a restoring force and is coupled to the Alfvén waves. The solid crust ranges from $z = -d$ to the surface $z = 0$. The depth d of the outer crust is given by $d \approx 10^5$ cm. Our consideration is limited to the thin outer crust only. A slab geometry is valid there because $d \ll R$. The gravitational acceleration in this region is almost constant and is approximated as $-g\boldsymbol{e}_z$, with $g = 10^{14}$ cm s^{-2}. The density distribution $\rho(z)$ is given by the integration of a hydrostatic equation for the neutron star crust ($|z| < d$), where degenerate electron pressure is dominant. The analytic expression of this is available as (Blaes et al. 1989)

$$\rho = 8.0\times10^1 \left[(|z|/\mathrm{cm}) + 2.5\times10^{-4}(|z|/\mathrm{cm})^2\right]^{3/2} \mathrm{g\ cm^{-3}}. \quad (1)$$

This explicit form will be used for the numerical calculations in the subsequent sections.

2.2. *Wave Equation*

We consider the propagation of shear Alfvén waves on the basis of linearized perturbation theory. In the deep interior, the gravitational force is so large that displacements to the vertical direction are not easily induced. The horizontal displacements of the disturbances are likely to be dominant, and they are coupled with the Alfvén waves. Some restrictions are imposed on the displacement vector $\boldsymbol{\xi}$ of the materials in order to extract the waves coupled with shear and magnetic stress. The waves propagating along the z-axis are assumed to satisfy $\xi_z = \nabla\cdot\boldsymbol{\xi} = 0$. This means that the waves are transverse and are decoupled from the compressional modes. The Lagrangian perturbations of density and pressure are zero because they are proportional to $\nabla\cdot\boldsymbol{\xi}$, i.e., $\Delta\rho/\rho = -\nabla\cdot\boldsymbol{\xi} = 0$, and $\Delta p/p = -(\partial \log p/\partial\log\rho)_{ad}\nabla\cdot\boldsymbol{\xi} = 0$.

The general forms of the displacements can be expressed by Fourier and Bessel functions with respect to time and cylindrical radius, respectively. We further simplify the displacements by assuming nodeless functions in a cylindrically radial direction, i.e., neglecting the radial structure. The regular form near the z-axis is given simply in cylindrical coordinates (ϖ, ϕ, z) by

$$\boldsymbol{\xi} \propto (\boldsymbol{e}_\varpi \pm i\boldsymbol{e}_\phi)\varpi^{m-1}\xi_{\pm m\omega}(z)e^{-i(\omega t \mp m\phi)}, \quad (2)$$

where m is a positive integer, $m \geq 1$. The mode of the helicity of the upper sign in equation (2) is positive, whereas that for the lower sign is negative. We can limit the Fourier mode to a certain frequency region, using the general relation $\xi_{\pm m-\omega} = \xi^*_{\mp m\omega}$, where the asterisk indicates a complex conjugate. We define the frequency in the corotating frame $\sigma_\pm \equiv \omega \mp m\Omega$ for each helicity state $\xi_\pm$ and limit the range to $\sigma_\pm \geq 0$. From now on, we omit the suffixes $m\omega$ in order to avoid complicated notations. Displacement (2) satisfies $(\nabla\times\boldsymbol{\xi})_z = 0$ and is therefore decoupled from the vorticity, as desired. The displacement corresponding to $m = 1$ has a clear meaning and can be written in Cartesian coordinates as $\boldsymbol{\xi} = (\boldsymbol{e}_x \pm i\boldsymbol{e}_y)\ \xi_\pm e^{-i\omega t}$. This mode represents uniform motion in the horizontal direction. A slightly different treatment is necessary for the axially symmetric perturbation $m = 0$. The regular displacement satisfying the above conditions is given as $\boldsymbol{\xi} = \xi_\phi(t,\varpi)\varpi\boldsymbol{e}_\phi$, which corresponds to the velocity perturbation $\delta\boldsymbol{e} = (\partial\xi_\phi/\partial t)\varpi\boldsymbol{e}_\phi \equiv \delta\Omega\varpi\boldsymbol{e}_\phi$. This kind of perturbation merely represents the impulsive jump of angular velocity as $\Omega \to \Omega + \delta\Omega$ and is not considered further in this paper.

The restoring forces for the modes are elastic shear stress δS_i and electromagnetic force δF_i. The linearized equation of motion can be written as

$$\rho\left[\frac{\partial}{\partial t}\delta v_i + (\boldsymbol{v}\cdot\nabla)\delta v_i + (\delta\boldsymbol{v}\cdot\nabla)v_i\right] = \delta S_i + \delta F_i, \quad (3)$$

where $\boldsymbol{v} = \varpi\Omega\boldsymbol{e}_\phi$ and the relation between the displacement and velocity perturbation is

$$\delta v_i = \frac{\partial}{\partial t}\xi_i + (\boldsymbol{v}\cdot\nabla)\xi_i - (\boldsymbol{\xi}\cdot\nabla)v_i. \quad (4)$$

The shear stress δS_i associated with deformation is

$$\delta S_i = \nabla_j\left[\mu\left(\frac{\partial\xi^i}{\partial x^j} + \frac{\partial\xi^j}{\partial x^i}\right)\right], \quad (5)$$

with shear modulus $\mu = 4.8\times10^{27}(\rho/10^{11}\ \mathrm{g\ cm^{-3}})^{4/3}$ ergs cm^{-3} (Baym & Pines 1971). The electromagnetic force is given by

$$\delta\boldsymbol{F} = \delta\rho_e\boldsymbol{E} + \rho_e\delta\boldsymbol{E} + \frac{1}{c}(\delta\boldsymbol{j}\times\boldsymbol{B} + \boldsymbol{j}\times\delta\boldsymbol{B}). \quad (6)$$

The crust is a perfect conductor, so the electric fields for both unperturbed and perturbed states are induced by the material motion as

$$\boldsymbol{E} = -\frac{1}{c}(\boldsymbol{v}\times\boldsymbol{B}) = -\frac{\varpi\Omega B_0}{c}\boldsymbol{e}_\varpi, \quad (7)$$

$$\delta\boldsymbol{E} = -\frac{1}{c}(\delta\boldsymbol{v}\times\boldsymbol{B} + \boldsymbol{v}\times\delta\boldsymbol{B}). \quad (8)$$

The electric charge and current of the unperturbed state are

$$\rho_e = -\frac{1}{2\pi c}\Omega B_0, \quad \boldsymbol{j} = \rho_e\boldsymbol{v}. \quad (9)$$

Quantities (7) and (9) satisfy the force balance $\rho_e\boldsymbol{E} + \boldsymbol{j}\times\boldsymbol{B}/c = 0$. These expressions are valid in the region smaller than light cylinder, c/Ω, or the actual stellar radius, R. Otherwise, we would need a better approximation than the uniformly rotating cylindrical model. Therefore, our present model is adequate to the behavior near the z-axis. As is confirmed by the explicit forms of $\boldsymbol{E}$ and $\delta\boldsymbol{E}$, the first term in equation (6), $\delta\rho_e\boldsymbol{E}(= (\nabla\cdot\delta\boldsymbol{E}/4\pi)\boldsymbol{E}$, is proportional to $(\Omega\varpi/c)^2$ and is smaller than the other terms near the z-axis, i.e., for the region $\varpi^2 < \xi/\xi''$. We therefore neglect it in the propagation of Alfvén waves. Eliminating $\delta\boldsymbol{E}$ by equation (8), the Lorentz force (eq. [6]) is reduced to

$$\delta\boldsymbol{F} = \frac{1}{c}(\delta\boldsymbol{j} - \rho_e\delta\boldsymbol{v})\times\boldsymbol{B}. \quad (10)$$

The perturbation of electric current is determined by the Maxwell equations

$$\nabla \times \delta \boldsymbol{E} = -\frac{1}{c}\frac{\partial}{\partial t}\delta \boldsymbol{B}, \tag{11}$$

$$\nabla \times \delta \boldsymbol{B} = \frac{4\pi}{c}\delta \boldsymbol{j} + \frac{1}{c}\frac{\partial}{\partial t}\delta \boldsymbol{E}. \tag{12}$$

From equations (8) and (11), the perturbations of electromagnetic fields are expressed in terms of the displacement vector as

$$\delta \boldsymbol{B} = B_0 \nabla_z \boldsymbol{\xi} = B_0 \varpi^{m-1}\frac{d\xi_\pm}{dz}(\boldsymbol{e}_\varpi \pm i\boldsymbol{e}_\phi)e^{-i(\omega t \mp m\phi)}, \tag{13}$$

$$\delta \boldsymbol{E} = \frac{B_0 \varpi^{m-1}}{c}\left[\mp(\omega \mp m\Omega)\xi_\pm(\boldsymbol{e}_\varpi \pm i\boldsymbol{e}_\phi) + \Omega\varpi\frac{d\xi_\pm}{dz}\boldsymbol{e}_z\right]e^{-i(\omega t \mp m\phi)}. \tag{14}$$

The stellar rotation induces the z-component of the perturbed electric field, which is important for angular momentum transfer, as discussed in § 2.6. Using these expressions and eliminating $\delta \boldsymbol{j}$ by equation (12), equation (3) is eventually reduced to

$$\frac{d}{dz}\left(\mu + \frac{B_0^2}{4\pi}\right)\frac{d}{dz}\xi_\pm + V_\pm \xi_\pm = 0, \tag{15}$$

where

$$V_\pm = \left(\rho + \frac{B_0^2}{4\pi c^2}\right)(\omega \mp m\Omega)[\omega \mp (mh-2)\Omega], \tag{16}$$

$$h = \frac{4\pi c^2 \rho}{4\pi c^2 \rho + B_0^2}. \tag{17}$$

2.3. *Propagation*

The propagation of Alfvén waves is studied in different astrophysical objects. Within certain parameters, our basic equation (15) should reduce to one previously studied. In the limit of the nonrotating case, equation (15) is reduced to the equation found by Blaes et al. (1989). The term $V_\pm$ is independent of the helicity state and is positive definite in this case. Another interesting limit of equation (15) is obtained when both the shear and relativistic effects are neglected. This limit corresponds to $\mu \to 0$ and $c^2 \to \infty$. In this case, the term $V_\pm$ becomes negative for a certain frequency region. Hence, the modes are nonpropagating (evanescent; see, e.g., Chandrasekhar 1961). We discuss the evanescent property below.

We consider the short-wavelength limit in order to see whether or not the waves propagate. The local dispersion relation is obtained by setting $\xi_\pm \propto e^{ikz}$ in equation (15) as

$$-v^2k^2 + (\omega \mp m\Omega)(\omega \mp (mh-2)\Omega) = 0, \tag{18}$$

where v is the velocity, defined as

$$v = c\left(\frac{4\pi\mu + B_0^2}{4\pi\rho c^2 + B_0^2}\right)^{1/2}. \tag{19}$$

In the limit of $\mu \to 0$ and $c^2 \to \infty$, the classical Alfvén wave velocity is recovered, i.e., $v = B_0/(4\pi\rho)^{1/2}$. The shear acts as a restoring force deep in the crust unless $B_0 \gg 2\times 10^{14}$ G. The displacement current contributes to additional inertia and is always important near the surface, where the propagation velocity becomes c.

Solving equation (18) for the frequencies $\sigma_\pm \equiv \omega \mp m\Omega \geq 0$, we have

$$\sigma_\pm = \mp\left[1 + \frac{m}{2}(1-h)\right]\Omega + \left\{\left[1 + \frac{m}{2}(1-h)\right]^2\Omega^2 + v^2k^2\right\}^{1/2}. \tag{20}$$

We do not have to consider the modes with negative frequency, $\sigma_\pm < 0$, because of the correspondence $(\xi_\pm, \sigma) \leftrightarrow (\xi_\mp^*, -\sigma)$, as mentioned in § 2.2. The difference between the two helicity modes is clear in the weak magnetic field limit, i.e., $vk/\Omega \to 0$ and $h \to 1$. In this limit, the frequencies in the corotating frame are given by $\sigma_- \approx 2\Omega$ and $\sigma_+ \approx v^2k^2/(2\Omega)$. The mode ξ_- with frequency σ_- represents an inertial wave due to Coriolis force. On the other hand, the mode ξ_+ with smaller frequency $\sigma_+ (\ll \sigma_-)$ represents a drift wave. Our problem is limited to cylindrical geometry, but similar oscillations are also possible in spherical geometry. See, e.g., Levin & D'Angelo (2004) for comparison in the nonrelativistic limit, but note that careful treatment is necessary to convert the results between the different geometries.

Like the Alfvén waves in classical treatment, the waves with low frequencies become nonpropagating because of the Coriolis force. Mode ξ_+ always propagates as far as $\sigma_+ \geq 0$, whereas mode ξ_- is nonpropagating for the frequency region $0 \leq \sigma_-/\Omega \leq 2 + m(1-h)$. The condition becomes $0 \leq \sigma_-/\Omega \leq 2$ when relativistic effects are neglected. The evanescent property in our problem depends on the spatial position through $h(z)$, which is calculated for the density distribution (eq. [1]) and constant magnetic field strength B_0. In general, function h decreases from $h \sim 1$ in deep interior to $h \sim 0$ near the surface with low density. The evanescent region therefore prevails near the surface. In Figure 1 we demonstrate the location of the evanescent region using the local dispersion relation. The critical frequency $\sigma_-/\Omega = 2 + m(1-h)$ is shown. The depth of the evanescent region increases with azimuthal wave number m, as well as with magnetic field strength B_0.

The phase and group velocities of the shear Alfvén waves in the inertial frame are respectively given by $v_p = \omega/k$ and $v_g = \partial\omega/\partial k$. The following relation is easily calculated:

$$\frac{v_p v_g}{v^2} = \frac{\omega}{\omega \pm \frac{1}{2}[2 - m(1+h)]\Omega} = \frac{\sigma_\pm \pm m\Omega}{\sigma_\pm \pm \frac{1}{2}[2 + m(1-h)]\Omega}. \tag{21}$$

This shows an interesting property: the phase and group velocities of the mode ξ_- are opposite in the propagating direction for the frequency range $[2 + m(1-h)]\Omega < \sigma_- < m\Omega$, which is possible for $m \geq 3$. The lower bound comes from the condition for the wave propagation.

In Figure 2 we show $1/N^2 = \omega^2/(c^2k^2)$ as a function of $\sigma_-/\Omega = \omega/\Omega + m$, using the local dispersion relation (eq. [18]). Frequencies corresponding to negative values of $1/N^2$ indicate the evanescent region. Nonpropagating frequencies ares located in low-frequency region. We now consider the propagation of the negative helicity mode with $2 < \sigma_-/\Omega < m$. The mode propagates as a wave in deep interior and may leak through to the exterior. The amplitude of the outgoing wave becomes small as it passes through the evanescent region. It is important to know the magnitude. The

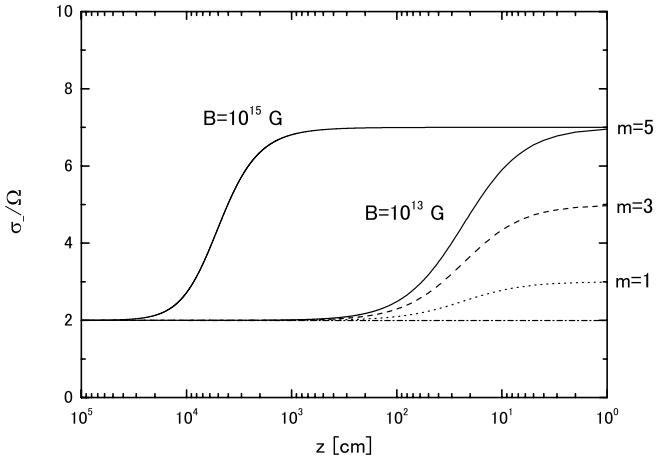


FIG. 1.—Critical angular frequency $\sigma_-/\Omega = 2 + m(1 - h)$ as a function of the depth from the surface. The evanescent region for negative helicity mode ξ_- is given by the condition $0 < \sigma_-/\Omega < 2 + m(1 - h)$. The critical frequencies are shown for $m = 1$, 3, and 5, with $B_0 = 10^{13}$ G and $m = 5$ with $B_0 = 10^{15}$ G. Note that the evanescent condition becomes $0 < \sigma_-/\Omega < 2$ (*dash-dotted line*) if all relativistic effects are neglected. The evanescent region near the surface enlarges with the increase of m and the magnetic field strength.

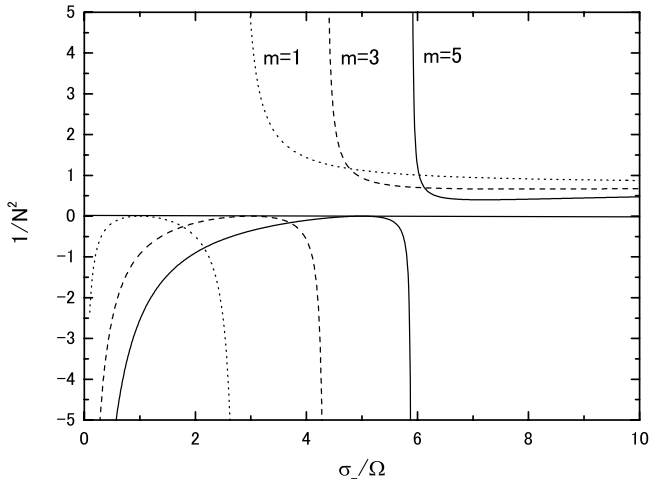


FIG. 2.—Dispersion relation of negative helicity mode ξ_- as a function of angular frequency σ_-/Ω at $z = 10$ cm from the surface.

damping rate depends on the frequency and the depth d_*. The exponential damping factor $e^{-\kappa d_*}$ is estimated as $\kappa d_* \approx |N|\omega d_*/c$, which is not so large, and in fact it is roughly $\sim 10^{-4}$ for large m. This means that the damping of the amplitude is not so significant, and therefore the disturbances of some modes penetrate to the surface.

2.4. *Exterior*

There are at least two possibilities for the exterior of the stars. One is that the plasma surrounding the star corotates with the same angular velocity. Such corotation occurs when the plasma is frozen in closed magnetic field lines. However, along open field lines the plasma freely moves to infinity, in which case the angular velocity is arbitrary. We consider this situation by assuming that the plasma exterior to the star is static in the inertial frame. A difference of the plasma motion in the background state is not so important for the high-frequency modes of the perturbations ($\omega \gg \Omega$), but it is crucial for the low-frequency modes, as discussed below.

When the plasma corotates with the same angular velocity, Ω, the perturbation equation corresponds to the limit of equation (15), with $\rho = \mu = 0$. A wave solution is possible for modes with $(\omega \mp m\Omega)(\omega \pm 2\Omega) > 0$, and the outgoing wave is expressed as

$$\xi_\pm = A_\pm \exp\,[ik_\pm z], \tag{22}$$

where

$$k_\pm = \frac{[(\omega \mp m\Omega)(\omega \pm 2\Omega)]^{1/2}}{c}. \tag{23}$$

We assume that the interior and exterior solutions are continuously matched, so that the boundary condition of the displacement at $z = 0$ can be expressed as

$$\frac{d\xi_\pm}{dz} = ik_\pm \xi_\pm. \tag{24}$$

We next consider nonrotating plasma exterior to the star. In this case, the outgoing boundary condition at the surface is replaced by

$$\frac{d\xi_\pm}{dz} = i\frac{\omega}{c}\xi_\pm. \tag{25}$$

The shaking of the magnetic field lines induces electromagnetic radiation in the exterior vacuum. Since $\delta B_z = 0$ everywhere, the perturbation should be matched with the transverse magnetic mode using the cylindrical wave guide (Jackson 1975). The perpendicular components of electric fields, i.e., $\delta E_\varpi, \delta E_\phi$ are continuous. They are expressed by $\boldsymbol{\xi}$ in the interior and vary as $\propto \exp[i\omega(z/c - t)]$ in the exterior. Thus at the surface we have the boundary condition shown in equation (25).

2.5. *Transmission Coefficient*

In this section we consider the extent to which Alfvén waves excited in the crust are transmitted to the exterior. We numerically solve equation (15) for the region from the deep interior $z \approx 10^5$ cm, corresponding to the neutron drip in the density, to the surface. The following asymptotic solution is obtained in the deep crust (Blaes et al. 1989). It is a sum of outgoing and reflecting waves, which respectively propagate to $+z$ and $-z$ directions. We normalize the amplitude of the outgoing waves to unity for simplicity and denote that of the reflecting waves by $R_\pm$.

$$\xi_\pm \approx |z|^{-7/4}\left\{\exp\left[i\int\frac{\Gamma_\pm}{v}\,dz\right] + R_\pm \exp\left[-i\int\frac{\Gamma_\pm}{v}\,dz\right]\right\}. \tag{26}$$

Here, $\Gamma_\pm$ is the effective frequency of each wave mode, defined as

$$\Gamma_\pm = \{(\omega \mp m\Omega)[\omega \mp (mh - 2)\Omega]\}^{1/2}. \tag{27}$$

The outgoing wave solution in the exterior is given by equation (22) with a transmission amplitude, $A_\pm$. We here assume that the exterior plasma corotates with Ω. The interior solution should be continuously matched with the exterior one

at the surface, $z = 0$. Thus, the transmission coefficients $T_\pm$ for each helicity mode are given by the relation

$$T_\pm = |A_\pm|^2 = 1 - |R_\pm|^2. \tag{28}$$

Our numerical calculation is limited to $m = 1$. The lower bound of the frequency for the positive helicity mode is $\sigma_+ > 0$, that is, $\omega > \Omega$. On the other hand, that for the negative helicity mode is limited by propagation condition $\sigma_- > 3\Omega$, that is, $\omega > 2\Omega$. In Figure 3 the transmission coefficients, $T_\pm$, for each helicity mode are shown as a function of the angular frequency in inertial frame ω. The rotational effect may be important in the millisecond magnetar model. In the calculation, the star is assumed to rotate with a constant angular velocity, $\Omega/(2\pi) = 10^3$ Hz. This value is somewhat too rapid for SGRs, but we can regard it as an extreme value that could be present during the newly born phase. The rotational effect becomes smaller for much smaller values of Ω. For comparison, we also show the result T_0 for the nonrotating case ($\Omega = 0$) by solid curves in Figure 3. The difference between the positive and negative helicity states is clear near the low-frequency limit, i.e., ω less than a few times Ω. The difference, however, becomes almost negligible in the high-frequency regime, say, $\omega > 10\Omega$. The transmission rates gradually approach unity with an increase of the frequency. The rates also increase with magnetic field strength, but $T_\pm \neq 1$ in the low-frequency regime even for 10^{15} G. A significant fraction of waves suffer from the bounce at the surface, because of $T_\pm \sim 0.1$ for $\omega < 10\Omega$. This means that the transmission time to the exterior is roughly estimated not by the crossing time d/v, but by $d/v \times T_\pm^{-1}$.

2.6. *Energy and Angular Momentum Loss*

We calculate the rate of energy and angular momentum carried by the Alfvén waves. The terms linear to the perturbation quantities vanish in the time average. Meaningful time-averaged values come from the square of the perturbation quantities. The time-averaged Poynting flux is therefore given by

$$\boldsymbol{S} = \frac{c}{8\pi}\Re(\delta\boldsymbol{E} \times \delta\boldsymbol{B}^*), \tag{29}$$

where the asterisk means a complex conjugate and $\Re(\ldots)$ means taking the real part. We have here used a useful technique in averaging the product of complex quantities with the same harmonics time dependence as shown in the textbooks (e.g., Jackson 1975). The power P radiated across the surface at $z = 0$ is calculated by integrating S_z over a circle within ϖ_*:

$$\begin{aligned} P &= \frac{c}{8\pi}\int_0^{\varpi_*}\int_0^{2\pi} \Re\Big(\delta E_\varpi^* \delta B_\phi - \delta E_\phi^* \delta B_\varpi\Big)\varpi\, d\varpi\, d\phi \\ &= \frac{(\omega \mp m\Omega)B_0^2 \varpi_*^{2m}}{4m}\Re\left(-i\xi_\pm^* \frac{d\xi_\pm}{dz}\right)_{z=0}. \end{aligned} \tag{30}$$

This is roughly estimated as $P \sim (\delta B)^2(\pi\varpi_*^2)c$. The power $P_{(R)}$ ejecting to the corotating ambient plasma is evaluated using boundary condition (24). The power $P_{(S)}$ to the static plasma is also calculated with condition (25). The explicit expressions are

$$P_{(R)} = \frac{(\omega \mp m\Omega)k_\pm B_0^2 \varpi_*^{2m}|\xi_\pm|_{z=0}^2}{4m}, \tag{31}$$

$$P_{(S)} = \frac{(\omega \mp m\Omega)\omega B_0^2 \varpi_*^{2m}|\xi_\pm|_{z=0}^2}{4mc}. \tag{32}$$

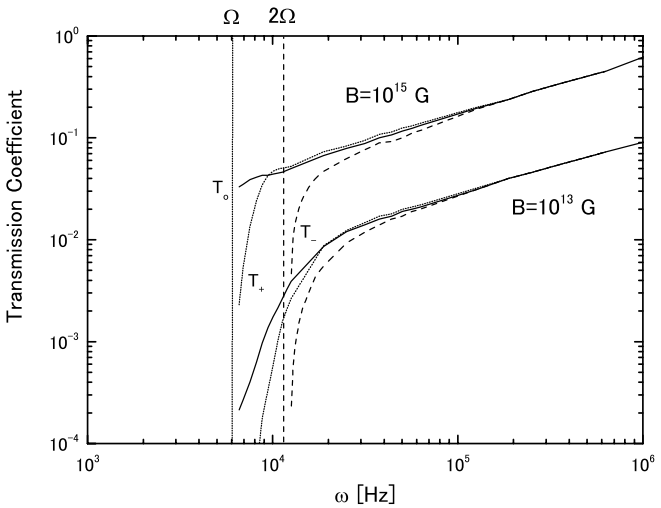


FIG. 3.—Transmission rates as a function of angular frequency for magnetic field strengths of 10^{13} and 10^{15} G. The curves labeled T_+ and T_- denote results for the positive and negative helicity states. The solid curves labeled T_0 denote results for a nonrotating star.

In a similar way, the angular momentum flux per unit time across $z = 0$ can be calculated. The transport of the angular momentum results in the torque. The time-averaged torque due to the electromagnetic stresses can be expressed in terms of the surface integral. From the symmetry, nonvanishing angular momentum flux is z-component only, which is expressed as

$$\begin{aligned} N_z &= -\frac{1}{8\pi}\int_0^{\varpi_*}\int_0^{2\pi} \Re\Big(\delta B_\phi^* \delta B_z + \delta E_\phi^* \delta E_z\Big)\varpi^2\, d\varpi\, d\phi \\ &= \frac{(\omega \mp m\Omega)\Omega B_0^2 \varpi_*^{2m+2}}{8(m+1)c^2}\Re\left(-i\xi_\pm^* \frac{d\xi_\pm}{dz}\right)_{z=0}. \end{aligned} \tag{33}$$

The angular momentum transfer in equation (33) comes from the electric part only, since $\delta B_z = 0$. The value is estimated as $N_z \sim (\Omega\varpi_*/c) \times (\delta B)^2 \varpi_*(\pi\varpi_*^2)$, and it is smaller by an extra factor $(\Omega\varpi_*/c)$ than the rough estimate that uses the magnetic part only. Note that the angular momentum transfer comes from the magnetic term, i.e., $B_\phi B_z$ for nonrelativistic case such as interstellar clouds. Depending on the boundary condition (eq. [24] or eq. [25]), the angular momentum flux is written as

$$N_{z(R)} = \frac{(\omega \mp m\Omega)k_\pm \Omega B_0^2 \varpi_*^{2m+2}|\xi_\pm|_{z=0}^2}{8(m+1)c^2}, \tag{34}$$

$$N_{z(S)} = \frac{(\omega \mp m\Omega)\omega\Omega B_0^2 \varpi_*^{2m+2}|\xi_\pm|_{z=0}^2}{8(m+1)c^3}. \tag{35}$$

It should be noted that the angular momentum flux can be made negative by the waves going out into the static ambient plasma, as shown in equation (35). This is possible if the condition $(\omega \mp m\Omega)\omega = \sigma_\pm \omega < 0$ is satisfied, that is, if frequencies σ and ω are opposite in sign. This condition is the same as the criterion of gravitational radiation reaction instability (Friedman & Schutz 1978). The oscillation mode counterrotates when viewed in frame that rotates with the star but corotates when viewed in the inertial frame. This provides a mechanism for converting the stellar rotational energy into gravitational radiation. The modes satisfying the condition $(\omega \mp m\Omega)\omega < 0$ are very interesting. They carry negative

angular momentum. The emission leads to the spin-up of the star.

2.7. *Order of Magnitude*

There is a simple relation between the energy flux (eq. [30]) and the angular momentum flux (eq. [33]) exerted by the Alfvén waves:

$$N_z = \frac{m\Omega\varpi_*^2}{2(m+1)c^2}P. \tag{36}$$

This holds irrespective of the boundary condition (eq. [24] or eq. [25]). The total angular momentum loss/gain is related to the total energy radiated by the waves. During the waves emission, the stellar structure may change as a result of rearrangement of magnetic fields, and the inertial moment I may be modified. Such a possibility has been discussed for giant bursts in SGRs (Ioka 2001; Woods et al. 2001). We do not consider the possibility here. The duration time of the wave emission is denoted by τ. The change in the angular velocity $\Delta\Omega$ is expressed by the total energy $\Delta E_{\rm A} = P\tau$,

$$\frac{\Delta\Omega}{\Omega} = \frac{N_z\tau}{I\Omega} = \frac{m\varpi_*^2}{2(m+1)c^2I}\Delta E_{\rm A} \sim 10^{-20}\left(\frac{\varpi_*}{10^4\ {\rm cm}}\right)^2\left(\frac{\Delta E_{\rm A}}{10^{38}\ {\rm ergs}}\right), \tag{37}$$

where the total energy of the Alfvén waves is not known but is used for the typical burst energy observed in SGRs. There are reports of glitches observed in AXPs (Kaspi et al. 2003), $\Delta\Omega/\Omega \sim 10^{-6}$. Our estimate is too small. We can expect much larger total energy to be associated with the giant bursts. Even taking comparable energies observed in X-/γ-rays in such events, $\Delta E_{\rm A} \sim 10^{44}$ ergs, the change is $\Delta\Omega/\Omega \sim 10^{-14}$, whereas $|\Delta\Omega/\Omega| \sim 10^{-4}$ in the giant burst. One reason for this smallness may be that the situation is too idealized, in particular, in that our model gives $\delta B_z = 0$ exactly. This introduces a small factor, $(\Omega\varpi_*/c) \sim 10^{-6}$, into the angular momentum loss N_z. Moreover, larger values of ϖ_* are required. Otherwise, the wind of particles and MHD waves or interaction between the crustal neutron superfluid and the rest of the neutron star would be more efficient processes for angular momentum transfer (Thompson et al. 2000).

3. DISCUSSION

We have studied the propagation of shear Alfvén waves through the neutron star crust to the exterior. Using a simplified cylindrical model, some interesting features are found. Waves with high frequency, $|\omega/(m\Omega)| \gg 1$, always propagate, whereas those with low-frequency propagate or not depending on spatial position. The transmission coefficient, which depends on the helicity state, is explicitly calculated. The ejection rate to the exterior increases with the frequency of the wave and the magnetic field strength.

We now consider the behavior of modes in the low-frequency regime. The positive helicity modes, ξ_+, always propagate as far as $\sigma_+ > 0$, whereas the negative helicity modes, ξ_-, become evanescent near the surface for $0 < \sigma_- < (m+2)\,\Omega$. If a corotating plasma covers the surface, the disturbances do not propagate in the atmosphere. On the other hand, if such a plasma does not exist, i.e., in the static plasma or vacuum cases, then the perturbations revive as outward waves in the exterior, although they suffer from some damping as they pass through the interior evanescent region. The exponential decay of the amplitude is not so large, for $\sigma_- \sim m\Omega$ with large m, as shown in § 2.3. The disturbances therefore penetrate to the surface and eventually escape to infinity.

When waves with frequency $0 < \sigma_- < m\Omega$ are ejected, they carry away negative angular momentum through the surface. In this case, the torque becomes positive and leads to a spin-up of the star by the outgoing waves. However, the magnitude is not enough to explain the glitches observed in AXPs (Kaspi et al. 2003). Geometrical factors may be important in the actual situation. In our model, the spin axis agrees with the direction of wave propagation, and the direction of the perturbations is orthogonal to the spin axis. For magnetic field lines misaligned with the rotation axis, the direction of the perturbations is perpendicular to the propagation, but not to the spin axis. In this case, δB_z is induced in general, and the nonvanishing term $\delta B_\phi \delta B_z$ results in larger torque (see eq. [33] and discussion). Compressional fast/slow magnetosonic waves are also induced at the same time. These calculations would be much more complicated.

The increase of angular momentum as the result of radiation is very analogous to that in the gravitational radiation reaction instability, i.e., the so-called CFS mechanism (Chandrasekhar 1970; Friedman & Schutz 1978). The generic criterion of the instability is $\sigma_\pm\omega < 0$ for unmagnetized rotating stars. Some fluid oscillation modes satisfying this condition can grow within a secular timescale as a reaction of gravitational radiation. The low-frequency mode satisfies the instability criterion. Related to this, there is a suggestive work by Ho & Lai (2000). They considered r-mode instability driven by Alfvén wave emission as well as gravitational wave emission. As for the dimensional estimate, the transfer rate by Alfvén waves is larger than that by gravitational waves for highly magnetized stars, $B \geq 3\times10^{12}(T/10\ {\rm ms})^{-3}$ G. They pointed out that Alfvén wave–driven instability is an efficient process. In their treatment, however, the displacement current is neglected, and hence the dynamical degree of the electromagnetic fields is eliminated in a sense. Such an approximation may be justified in the deep interior, but not near the surface. Our treatment concentrates on the crust, not the interior core, the bulk motion of which is important for estimating gravitational radiation. Thus a global calculation adequate for the emission of both gravitational and Alfvén waves is required to determine the most efficient mechanism.

As for the fundamental problem of the secular instability, the criterion should be clarified by taking into account strong magnetic fields. For example, Friedman & Schutz (1978) constructed a canonical energy relevant to the instability only for unmagnetized stars. In their treatment of secular instability, the effect of gravitational emission is neglected in dynamical equations, but it should be accounted for in the energy equation governing evolution on a longer timescale. Our problem differs on this point. The degree of freedom of the electromagnetic fields is accounted for in the dynamical equation, and hence Alfvén wave emission from the surface is inevitably included. There is no mathematically rigorous proof of the secular stability criterion in magnetized stars, so further study is necessary to examine the possibility of unstably growing modes coupled with electromagnetic fields.

Finally, we comment on some problems in applying more realistic models relevant to magnetars. The rotation of observed magnetars is very slow $\Omega \sim 1$ rad s^{-1}. In order to satisfy the condition $0 < \sigma_- < m\Omega$, a large azimuthal number, say $m \sim 10^3$, is needed. If there are rapidly rotating stars, a moderate value of m may be sufficient. The other important

factor is the magnetic configuration. Thompson et al. (2002) considered a magnetosphere threaded by a large-scale electric current. The magnetic field structure is twisted and quite different from our present model. The perturbations of such magnetic fields are induced by bursts, and Alfvén waves propagate. However, the detailed treatment seems to be complicated, and highly numerical calculations are needed. We expect that the behavior of short wavelengths, say, much smaller than the curvature of the magnetic field, may be almost the same as given here. The result of the transmission rate calculated in § 2.5 may be relevant. For the long wavelength mode, geometrical effects are important and further studies are required.

This work was supported in part by Grants-in-Aid for Scientific Research (14047215, 16029207, and 16540256) from the Japanese Ministry of Education, Culture, Sports, Science, and Technology.

REFERENCES

Baym, G., & Pines, D. 1971, Ann. Phys. 66, 816
Blaes, O., Blandford, R., Goldreich, P., & Madau, P. 1989, ApJ, 343, 839
Carroll, B. W., Zweibel, E. G., Hansen, C. J., McDermott, P. N, Savedoff, M. P., Thomas, J. H., & Van Horn, H. M. 1986, ApJ, 305, 767
Chandrasekhar, S. 1961, Hydrodynamic and Hydromagnetic Stability (London: Oxford Univ. Press)
———. 1970, Phys. Rev. Lett. 24, 611
Cheng, B., Epstein, R. I., Guyer, R. A., & Young, A. C. 1996, Nature, 382, 518
Friedman, J. L., & Schutz, B. F. 1978, ApJ, 222, 281
Gavriil, F. P., Kaspi, V. M., & Woods, P. M. 2002, Nature, 419, 142
Göğüş, E., et al. 1999, ApJ, 526, L93
———. 2000, ApJ, 532, L121
Ho, W. C. G., & Lai, D. 2000, ApJ, 543, 386
Ibrahim, A. I., Swank, J. H., & Parke, W. 2003, ApJ, 584, L17
Ioka, K. 2001, MNRAS, 327, 639
Jackson, J. D. 1975, Classical Electrodynamics (New York: Wiley)
Kaspi, V. M., Gavriil, F. P., Woods, P. M., Jensen, J. B., Roberts, M. S. E., & Chakrabarty, D. 2003, ApJ, 588, L93
Kouveliotou, C., et al. 1998, Nature, 393, 235
Levin, Y., & D'Angelo, C. 2004, preprint (astro-ph/0403014)
Lyutikov, M., Thompson, C., & Kulkarni, S. R. 2002, in ASP Conf. Ser. 271, Neutron Stars in Supernova Remnants, ed. P. O. Slane & B. M. Gaensler (San Francisco: ASP), 262
Mereghetti, S., & Stella, L. 1995, ApJ, 442, L17
Shu, F. H. 1992, The Physics of Astrophysics (Mill Valley: University Science Books)
Thompson, C., 2000, The Neutron Star–Black Hole Connection, ed. V. Connaughton et al. (Dordrecht: Reidel)
Thompson, C., & Duncan, R. C. 1993, ApJ, 408, 194
———. 1995, MNRAS, 275, 255
———. 1996, ApJ, 473, 322
Thompson, C., Duncan, R. C., Woods, P. M., Kouveliotou, C., Finger, M. H., & van Paradijs, J. 2000, ApJ, 543, 340
Thompson C., Lyutikov, M., & Kulkarni, S. R. 2002, ApJ, 574, 332
Woods, P. M. 2004, Adv. Space Res., 33, 630
Woods, P. M., Kouveliotou, C., Göğüş, E., Finger M. H., Swank, J., Smith, D. A, Hurley, K., & Thompson, C. 2001, ApJ, 552, 748